Journal of Materials Science: Materials in Electronics (2019) 30:4688–4695
https://doi.org/10.1007/s10854-019-00762-x

Microstructures and electrical properties of Mn/Co/Ni-doped $BaBiO_3$ perovskite-type NTC ceramic systems

Jing-Jing Qu[1,3] · Xv-Qiong Li[2] · Fei Liu[1,2] · Chang-Lai Yuan[2] · Xiao Liu[2] · Hui-Wang Ning[1] · Hai-Lin Li[1]

Received: 23 November 2018 / Accepted: 16 January 2019 / Published online: 30 January 2019

Abstract
Mn/Co/Ni-modified $BaBiO_3$-based negative temperature coefficient (NTC) ceramics with the formula, x[(3-y-z)Mn/yCo/zNi-ions]+(1−x)$BaBiO_3$ (x = 0.0–0.4, y = 0.96 and z = 0.48), were synthesized using a conventional solid state reaction. The effects of Mn/Co/Ni-substitute content on the phase structures and composition, microstructures and electrical properties were characterized by X-ray diffraction (XRD), scanning electron microscope and resistance–temperature measurements, respectively. XRD pattern analysis results revealed that the compound phases consisted of a main monoclinal $BaBiO_3$ phase and a secondary phase of Ba(Mn, Co, Ni)O_3 solid-solution with a hexagonal structure, which were detected at x = 0.05–0.2. In addition, according to the XRD patterns, the main phase changed from $BaBiO_3$ to a rhombohedral $Bi_{8.11}Ba_{0.89}O_{13.05}$ phase at x = 0.3, and this phase content increased dramatically as the x value increased to 0.4. For the related electrical properties, all of the samples demonstrated the typical characteristics of NTC thermistors across a relatively wide range of temperatures. The values obtained for B constant ($B_{25/85}$) and the room-temperature resistivity (ρ_{25}) were in the range of 2297–5235 K and 760 Ω cm^{-1}, 620 kΩ cm, respectively, which implied that the electrical properties of the present ceramic systems could be optimized via various substitutions in the Mn/Co/Ni-ions content. The variable values of ρ_{25} were affected strongly by the changes in crystal structure and the decrease in charge carrier concentration. These composite ceramic materials are suitable candidates for a variety of NTC thermistor applications due to their widely adjustable electrical properties.

1 Introduction

Due to their advantages of high sensitivity, high precision, good reliability and capability for use directly in air, etc., spinel-structure oxides consisting of transition metals based on Mn–Co–Ni–O compounds are used in negative temperature coefficient (NTC) thermistor ceramics [1, 2], and as such have been widely studied for various industrial and domestic applications [3–5]. These NTC thermistors are extensively used in temperature measurement, control and compensation; circuit and electronic component protection; and flow rate and radiation measurement-related instruments [6, 7]. It is well known that the classical and excellent electrical characteristics of Mn–Co–Ni–O NTC thermistors are derived from the extensive electrical hopping conduction that occurs within the same cations with different valence states in the AO_4 (A = Ni and Co) and BO_6 (B = Mn) sites [8–10]. These characteristics depend on the following conductance mechanisms,

$$Ni^{2+} + Co^{3+} \leftrightarrow Ni^{3+} + Co^{2+} \quad (1)$$

$$Ni^{2+} + Co^{4+} \leftrightarrow Ni^{3+} + Co^{3+} \quad (2)$$

$$Ni^{2+} + Ni^{3+} \leftrightarrow Ni^{3+} + Ni^{2+} \quad (3)$$

$$Co^{2+} + Co^{3+} \leftrightarrow Co^{3+} + Co^{2+} \quad (4)$$

$$Co^{4+} + Co^{3+} \leftrightarrow Co^{3+} + Co^{4+} \quad (5)$$

$$Mn^{4+} + Mn^{3+} \leftrightarrow Mn^{3+} + Mn^{4+} \quad (6)$$

✉ Xv-Qiong Li
lixuqiong@guet.edu.cn

✉ Fei Liu
liufeiguet@163.com

[1] School of Mechanical and Electrical Engineering, Guilin University of Electronic Technology, Guilin 541004, People's Republic of China

[2] Guangxi Key Laboratory of Information Materials, Guilin University of Electronic Technology, Guilin 541004, People's Republic of China

[3] Department of Computer Science and Engineering, Guilin University of Aerospace Technology, Guilin 541004, People's Republic of China

which result in charge transitions where the small polaron hopping model is commonly proposed for the electrical conduction of the $(Mn_{3-y-z}Co_yNi_z)O_4$ spinel-structure systems [11, 12]. In particular, $Mn_{1.56}Co_{0.96}Ni_{0.48}O_4$ has been proven to be an important composition in some previous works [13–15]. This is attributed to the fact that this composition exhibits better electrical and stress transfer properties for the appropriate resistance and high temperature coefficient of resistance. This phenomenon is mainly due to the small-polaron hopping between the localized Mn^{3+}/Mn^{4+} and/or Mn^{4+}/Mn^{3+} valence states transition [Eq. (6)] under the assistance of thermal activation [16], which is regarded as an electron jump among adjacent cations of the same type with different valence states as well. The electrical conductivity attains a maximum value as the number of trivalent cations is equal to that of quadrivalent cations [17]. In addition, the main electrical characteristics of NTC ceramics are the thermal constant (B) and the room temperature resistivity (ρ_{25}); where in fact, the B constant indicates a sensitivity to temperature excursions. Some previous research results on NTC ceramics are shown in Table 1. With regard to the electrical properties, it should be pointed out that a large proportion of spinel-structure and some perovskite-structure thermistor ceramic systems have good temperature sensitivity and fast response, but a higher and narrower adjustable range for room temperature resistance as well, which probably limits their further development in diversified electrical/electronic devices [18–22]. With the further development of electronic information technology and digitization, new requirements have been put forward for NTC thermistor materials sintered at a lower temperature [15, 17], such that their use within a wide temperature range with a widely adjustable room temperature resistance have gradually entered mainstream research [23, 24].

$BaBiO_3$ with a monoclinic crystal structure is supposed to exhibit a metallic behavior as predicted by the theoretical calculation, yet it actually demonstrates semiconducting behavior [25]. Very few studies on the NTC characteristics of $BaBiO_3$-based ceramics including solid solutions and complex-phase systems have been reported up to now. In our early research [26, 27], an appropriate amount of Sb substitution for the Bi-site in $BaBi_{1-x}Sb_xO_3$ solid solutions revealed good electrical properties (large adjustable resistance range and high sensitivity constant) over a wide temperature scale. This can be explained by the fact that the Bi ions with different valence states, namely as Bi^{3+} and Bi^{5+}, in a tilting-mode lattice distortion of BiO_6 octahedra led to different energy level effects in electrical hopping conduction.

Based on the above analysis, in order to obtain electrical properties with widely adjustable room-temperature resistivity (ρ_{25}) and B constant in the given measured temperature range, we have synthesized thermistor ceramics through Mn/Co/Ni doping in $BaBiO_3$ (high conductivity phase) to form a solid solution or composite ceramics in the present work. Additionally, the influence of Mn/Co/Ni additions on the phase structures and content, microstructures and NTC electrical properties of the Mn/Co/Ni-modified $BaBiO_3$-based ceramic systems was also investigated systematically.

2 Experimental procedure

The high-purity oxide and/or carbonate of Mn_3O_4 (purity > 99.5%), Co_3O_4 (purity > 99.5%), NiO (purity > 99.9%), Bi_2O_3 (purity > 99.5%) and $BaCO_3$ (purity > 99.0%) were weighed in appropriate proportions to fabricate x[(3-y-z)Mn/yCo/zNi-ions]+(1 − x)$BaBiO_3$ (x = 0.0–0.4, y = 0.96 and z = 0.48) composite ceramics. The weighed powders were mixed and milled for 12 h in ethanol using zirconia balls in a high energy planetary ball mill. The ball-milled slurries were dried at 100 °C in an oven for 6 h, and then the dried powders were ground, sieved and calcined at 550 °C for 2 h. The calcined mass was crushed and ground in a mortar for 1 h to acquire a fine powder. Next, the fine composite ceramic powders were granulated with 7 wt.% PVA solution as an organic binder, and pressed into disks that were 11.5 mm in diameter and about 2.5 mm

Table 1 Recent research results for NTC thermistor ceramics

Year	Compositions	Sintering temperature (°C)	ρ_{25}(Ω cm)	B (K)	Ref.
2018	$MnFe_{1.95}Mo_{0.05}O_4$	1200	1.39×10^5	6353	[18]
2017	$NiMn_2O_4$	1200 + 900 (two-step sintering)	3.292×10^3	3550	[19]
2016	$(LaMn_{0.5}Co_{0.5}O_3)_x-(Ni_{0.66}Mn_{2.34}O_4)_{1-x}(0\le x\le0.5)$	1250	$4.767\times10^{3-20}$	3970–1573	[20]
2015	$Ni_{0.6}Mn_{2.3}Ti_{0.1}O_4$	1150	1.90×10^4	4225	[21]
2015	$Ni_{0.6}Mn_{2.1}Ti_{0.3}O_4$	1250	1.63×10^5	4594	[21]
2013	$0.6Y_2O_3-0.4YCr_{0.5}Mn_{0.5}O_3$	1600	5.683×10^6	3627	[22]
2013	$0.6Y_2O_3-0.4YCr_{0.5}Mn_{0.5}O_3+0.2$ wt% La_2O_3	1600	3.773×10^5	3681	[22]

in thickness under 220 MPa for 60 s to enhance the green body density. The ceramic composite disks were preheated at 550 °C for 1 h to expel the binder and further sintered in a furnace at 750 °C and/or 780 °C for 2 h in the air, respectively. In addition, the sintered disks were carefully polished into a thickness of approximately 1.0 mm. Finally, in order to study the electrical properties, Ag pastes were coated on both parallel sides of the polished samples, and after drying the pastes at room temperature, the disks specimens were heated at 620 °C for 30 min to make the electrodes.

X-ray diffraction (XRD) patterns were employed to understand the crystallographic information of the sintered ceramic samples using an X-ray powder diffractometer (D8-2-Advanced, Bruker AXS, Germany) equipped with Cu$K\alpha$ ($\lambda = 1.5406$ Å) radiation at a scanning rate of 5°/min. The microstructural features of the sintered ceramics were observed by scanning electron microscope (SEM, S-4800, Hitachi, Japan) in combination with an energy dispersive spectrometer (EDS). The temperature dependence of the resistivity (ρ–T) of the disk samples was measured in the temperature range of 25–300 °C using a resistance–temperature measurement system (ZWX-C, China) in the direct current (DC) condition, wherein the accuracy of the furnace measurements was ± 0.5 °C. Moreover, the B constant, called the coefficient of temperature sensitivity, was strongly influenced by the activation energy for hopping conduction (E_a) [6, 22], indicating a sensitivity to temperature excursions. The B value was calculated by Eq. (7):

$$B = \frac{T_1 \cdot T_2}{T_1 - T_\partial} \cdot ln\left(\frac{R_1}{R_2}\right) \tag{7}$$

where R and T were resistance and absolute temperature, respectively. In this work, $B_{25/85} = 1778.07 \cdot \ln(\rho_{25}/\rho_{85})$ [21], in which ρ_{25} and ρ_{85} were the resistivity at 25 °C and 85 °C, respectively.

3 Results and discussion

The x(1.56Mn/0.96Co/0.48Ni-ions) doped in $(1-x)BaBiO_3$ ceramic samples (abbreviated as xMn/Co/Ni + $(1-x)$ $BaBiO_3$) can be sintered to be relatively dense at a temperature of 780 °C/2 h at $x = 0.0$ and 750 °C/2 h at $x = 0.05$–0.4, respectively. Figure 1a shows the room-temperature XRD patterns of the $BaBiO_3$ ceramic sample sintered at 780 °C for 2 h and the xMn/Co/Ni + $(1-x)BaBiO_3$ ($x = 0.05$–0.3) ceramics sintered at 750 °C for 2 h, respectively. Through analysis with a Jade 6.5-PDF2008 program, it is clear that the conventionally sintered sample ($x = 0.0$) has a single monoclinic $BaBiO_3$ phase (PDF no. 35-1020) with a perovskite structure described by the space group C2/m (12). A small amount of $BaMnO_3$ phase (PDF no. 26–0168),

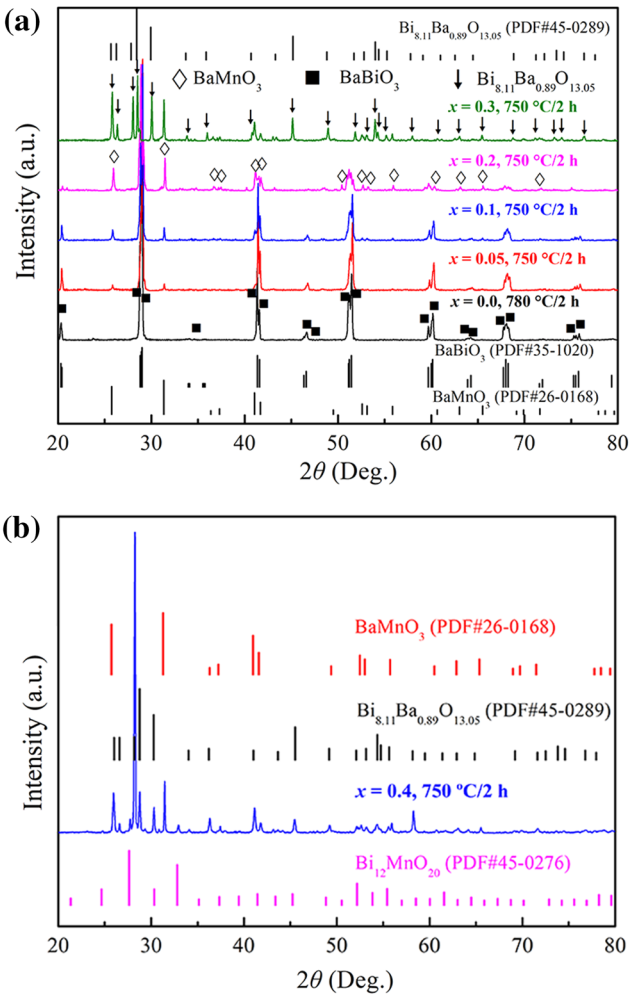

Fig. 1 **a** XRD patterns of as-sintered xMn/Co/Ni + $(1-x)BaBiO_3$ ($x = 0.0$–0.3) and **b** $x = 0.4$ composite ceramics

indexed as a hexagonal structure with the P63/mmc (194) space group, is detected at $x = 0.05$. Moreover, it is noted that the main diffraction peaks of the $BaMnO_3$ phase become sharper, and the intensity and number of the XRD peaks also increase when the x value increases to 0.2. As noted in the patterns of these samples ($x = 0.05$, 0.1 and 0.2), in addition to the main phase $BaBiO_3$ and second phase $BaMnO_3$, no other impurity phase can be observed. This indicates that the majority of Co- and Ni-ions substitutes are inclined to enter the perovskite lattice at the Mn-sites rather than the Bi-sites to form solid solutions, as a result of the average B-site ion radius $Co^{2+}/Co^{3+}/Co^{4+}$ (0.053, CN = 6) and Ni^{2+}/Ni^{3+} (0.063 nm, CN = 6), which is less than that of Bi^{3+}/Bi^{5+} (0.09 nm, CN = 6) and similar to that of Mn^{3+}/Mn^{4+} (0.056 nm, CN = 6) [28]. Additionally, as the Mn/Co/Ni doped content increases up to 0.3, the amount of Ba(Mn, Co, Ni)O_3 phase isomorphic to $BaMnO_3$ increases continuously. However, the $BaBiO_3$ phase is not observed in the

XRD pattern of this sintered ceramic and the diffraction pattern of the main crystal phase can be assigned to a rhombohedral $Bi_{8.11}Ba_{0.89}O_{13.05}$ phase belonging to the R-3m(166) space group (PDF no. 45-0289), indicating a phase transition occurring in the case of $BaBiO_3$ compounds with high Mn/Co/Ni-substitutes. This illustrates that a further increase in the Mn/Co/Ni content can reduce the solubility limit of $BaBiO_3$-based ceramic systems, and these results also imply that Ba-ions easily form perovskite-type solid solutions with Mn-, Co- and Ni-ions, thus producing the $Bi_{8.11}Ba_{0.89}O_{13.05}$ phase. Another point to note is that the Mn–Co–Ni–O compounds have difficulty forming a spinel-structure phase at sintering temperatures below 1100 °C [15, 17].

The XRD pattern of the sample $x=0.4$ sintered at 750 °C for 2 h is shown in Fig. 1b. It can be seen that the major phases presented in this ceramic sample still remain the $Bi_{8.11}Ba_{0.89}O_{13.05}$ phase and $BaMnO_3$ phase, wherein the intensity of the main diffraction peaks increase fairly obviously for the $Bi_{8.11}Ba_{0.89}O_{13.05}$ phase, which further confirms that the Ba-ions are inclined to form a hexagonal perovskite phase isomorphic to $BaMnO_3$ with Mn-, Co- and Ni-ions. According to some previous works [29, 30], $BaBiO_3$ at room temperature has been pointed out as having a minimal charge transfer between the two B sites, occupied by Bi^{3+} and Bi^{5+}, respectively. In $Bi_{8.11}Ba_{0.89}O_{13.05}$, the valence states of bismuth are more stable at trivalence (+3), therefore, the Bi-ions change from the variable to the fixed valence state with the increase in Mn-, Co- and Ni-ions doping. In addition, a minor $Bi_{12}MnO_{20}$ (PDF no. 45-0276) phase with cubic structure can also be detected in the sample with $x=0.4$. This result also verifies that bismuth ions are stable in trivalent form, and the further increase in Mn-, Co- and Ni-ions substitutions has exceeded the solubility limit of Ba(Mn, Co, Ni)O_3 as well.

Typical scanning electron microscope (SEM) images of as-fired surfaces of the xMn/Co/Ni + $(1-x)BaBiO_3$ ($x=0.0$–0.4) ceramics sintered at different temperatures for 2 h are illustrated in Fig. 2. As shown in Fig. 2a, the homogeneous microstructures with a few pores are revealed in the sample with $x=0.0$. As $x=0.05$, the compactness is slightly improved as seen from the appearance of the features, compared with that of the $BaBiO_3$ matrix, as shown in Fig. 2b. In fact, according to Archimedes' principle, the apparent porosity of these as-sintered ceramics can be obtained, and the apparent porosity values for xMn/Co/Ni + $(1-x)BaBiO_3$ ceramics are approximatively 7.3%, 5.2%, 6.3%, 5.4%, 4.8% and 5.9% with $x=0.0$, 0.05, 0.1, 0.2, 0.3 and 0.4, respectively. In general, a lower porosity means a higher relative density, and a more dense microstructure will obtain better reproducibility of the electrical characteristics of the ceramics. With the x value increasing from 0.1 to 0.2, a different kind of grain shape for the small grain sizes below approximately 500 nm can be observed clearly in Fig. 2c, d, implying a second phase emergence for the composites in $x=0.1$–0.2. In addition, for the samples of $x=0.3$ and $x=0.4$, it is evident from Fig. 2e, f that two kinds of grain sizes and shapes are quite distinct. Especially for the sample with $x=0.4$, the major phase grains are large and irregularly shaped.

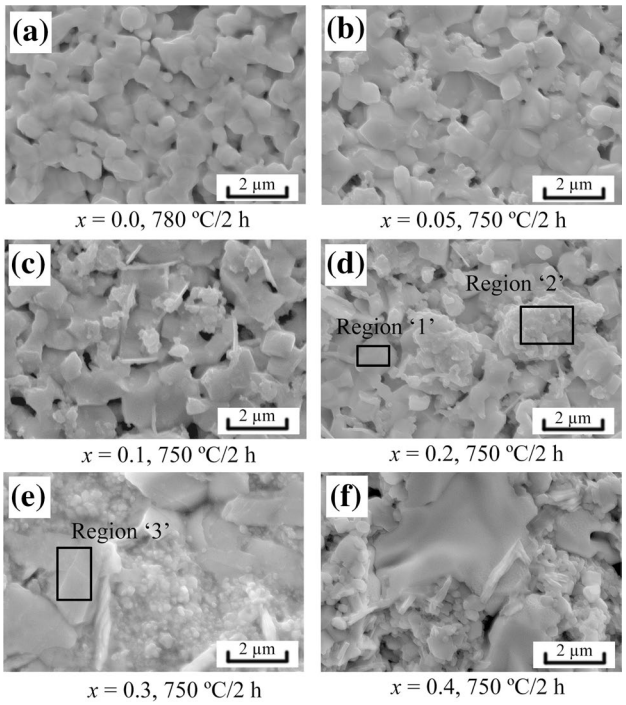

Fig. 2 High magnification SEM images of as-sintered xMn/Co/Ni + $(1-x)BaBiO_3$ ($x=0.0$–0.4) samples sintered at different temperatures for 2 h

To distinguish each kind of grain composition in these samples, energy dispersive spectrometer (EDS) analysis is carried out on the grains chosen from the specimens (regions '1'–'3', see Fig. 2d, e), as shown in Fig. 3. According to the related EDS analysis results of region '1' from Fig. 3a, the atom ratio of Ba and Bi and O is almost 1:1:3. The main phase grains are therefore confirmed to be $BaBiO_3$. Meanwhile, for the small grains detected in region '2', EDS data from the inset in Fig. 3b confirm that these agglomerated small grains are rich in Mn, Co, Ni and Ba, wherein the ratio of Mn/Ba and Ni/Ba is approximately 1:1. Moreover, there is almost no Bi element detected in region '2'. These results imply that a large proportion of Co- and Ni-ions substitutes are inclined to enter the perovskite lattice at Mn-sites, which also leads to the formation of Ba(Mn, Co, Ni)O_3 solid-solutions isomorphic to the $BaMnO_3$ phase more easily in the samples ($x=0.05$–0.2). On the other hand, from the EDS data of region '3' (see Fig. 3c), the atom ratio of Bi and Ba and O has only a small difference in the stoichiometry formula of $Bi_{8.11}Ba_{0.89}O_{13.05}$. Thus, the large and irregular

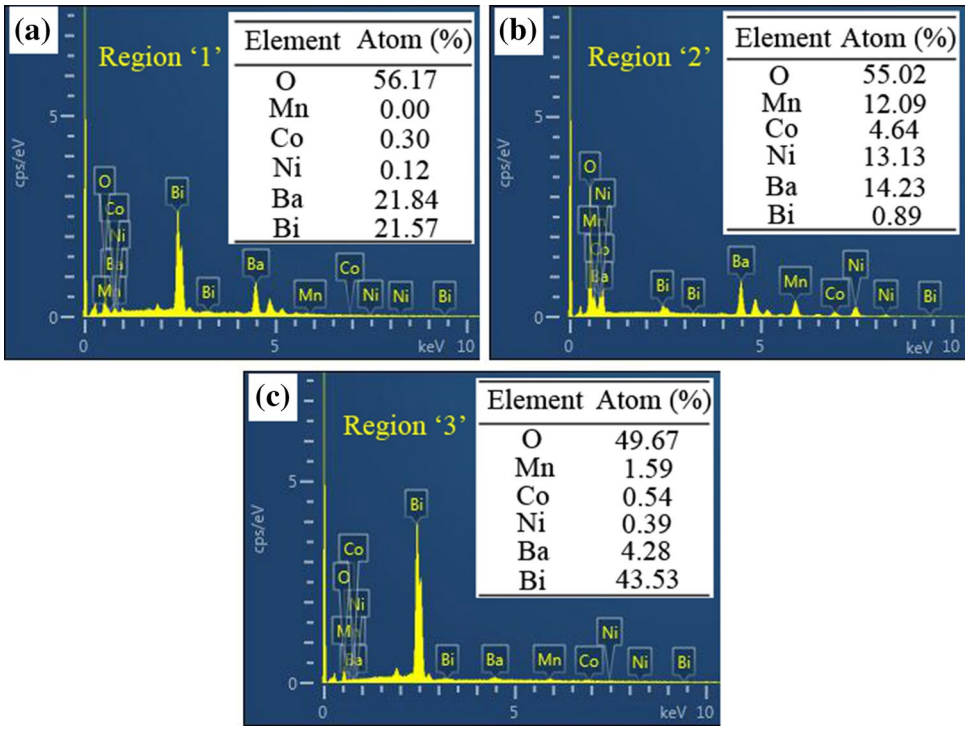

Fig. 3 EDS graphs and data of **a** region '1', **b** region '2' and **c** region '3' from the surfaces (in Fig. 2d, e) of xMn/Co/Ni + $(1-x)$$BaBiO_3$ ($x = 0.2$ and 0.3) ceramics sintered at 750 °C for 2 h

grains are proven to belong to the $Bi_{8.11}Ba_{0.89}O_{13.05}$ phase, in which a small amount of Mn, Co and Ni atoms dissolve on the grain surface. It is shown that the above analysis results are in good agreement with the results seen in the XRD patterns in Fig. 1.

Figure 4a displays the resistivity (ρ, calculated by DC resistance) versus temperature characteristics for xMn/Co/Ni + $(1-x)$$BaBiO_3$ ($x = 0.0$–0.4) ceramic samples in the temperature range of 25 °C to 300 °C. It can be seen clearly that all of the specimens show an exponential decrease in resistivity with the increase in the measured temperature over a relatively wide temperature range, and this represents the typical ρ–T curve of NTC thermistors [31]. Therein, the room-temperature resistivity (ρ_{25}) is approximately 1300 Ω cm, 760 Ω cm, 1770 Ω cm, 1950 Ω cm, 11,720 Ω cm and 1620 kΩ cm for the samples with $x = 0.0$, $x = 0.05$, $x = 0.1$, $x = 0.2$, $x = 0.3$ and $x = 0.4$, respectively. Here one can observe that the ρ_{25} value decreases as $x = 0.05$, and this is attributed to the decrease in porosity, compared with the sample where $x = 0.0$. The more dense ceramic body means a larger effective area in the grain-to-grain contact and a fewer number of insulating grain boundaries in the same volume of sample, resulting in the fact that the number of potential barriers at the grain boundaries encountered during electron conduction is also reduced, and the resistivity at room temperature is therefore decreased [19]. This result illustrates that a minor amount of Mn/Co/Ni-substitutes can promote densification and sintering for the high conductivity $BaBiO_3$ NTC thermistors. Additionally, it is observed that when the Mn/Co/Ni content increases from 0.05 to 0.2, the ρ_{25} value of xMn/Co/Ni + $(1-x)$$BaBiO_3$ begins to increase at the same sintering temperature. This is closely related to the increase in Ba(Mn, Co, Ni)O_3 phase content and the dragging effect [32]. It can be understood from the analysis above that the grain size of Ba(Mn, Co, Ni)O_3 solid-solution phase is relatively small and the grains are concentrated correspondingly. In addition, the different phase formations will lead to a barrier produced for the charge carriers, and thus the conductivity of the grains and grain boundaries are decreased as compared to the high conductivity $BaBiO_3$ grains [23]. As the amount of Mn/Co/Ni substitutes further increases, there is an extremely significant increase in the ρ_{25} values, especially for the sample with $x = 0.4$, which is strongly influenced by the changes in crystal structure. For the xMn/Co/Ni + $(1-x)$$BaBiO_3$ samples, the main crystalline phase transforms from a monoclinic $BaBiO_3$ phase into a rhombohedral $Bi_{8.11}Ba_{0.89}O_{13.05}$ phase as $x = 0.3$, and the phase content of $Bi_{8.11}Ba_{0.89}O_{13.05}$ has a substantial increase when the x value increases to 0.4. Therefore, the significantly increasing ρ_{25} values result from the fact that $Bi_{8.11}Ba_{0.89}O_{13.05}$ should be an insulator. In addition to this, as the amount of $Bi_{8.11}Ba_{0.89}O_{13.05}$ in the thermistors increases, the valence states of bismuth are more stable at trivalence (+3), leading to a sharp decrease in the amount of Bi^{3+}/Bi^{5+} charge carrier concentration and thereby increasing the resistivity at room temperature to a large extent as a result. However, the small polaron hopping between localized $Co^{2+}/Co^{3+}/Co^{4+}$, Ni^{2+}/Ni^{3+} and Mn^{3+}/Mn^{4+} states plays another important role in

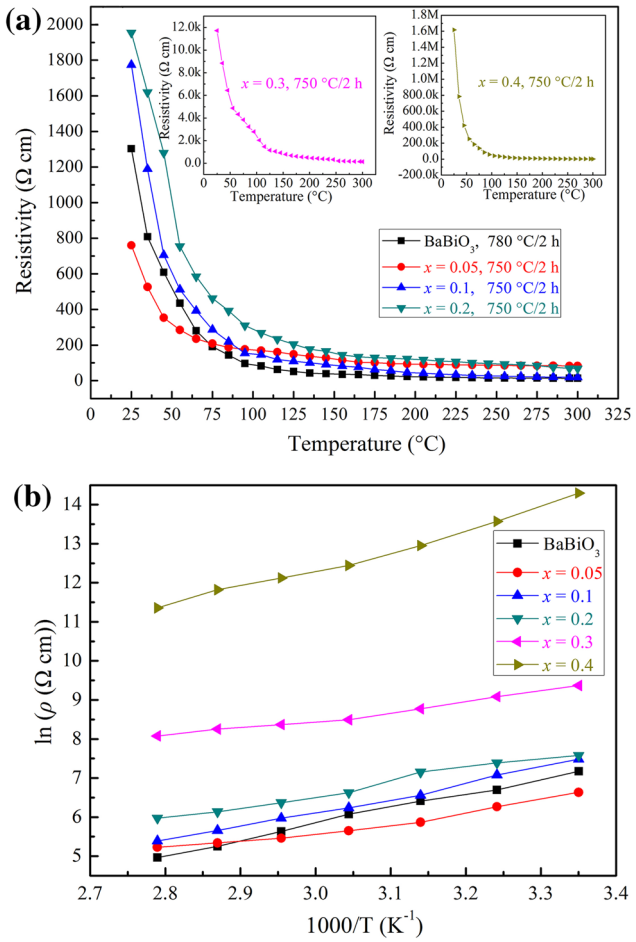

Fig. 4 **a** Relationship between the electrical resistivity and temperature and **b** Arrhenius plots of resistivity for as-sintered xMn/Co/Ni + $(1-x)$BaBiO$_3$ (x = 0.0–0.4) ceramic samples

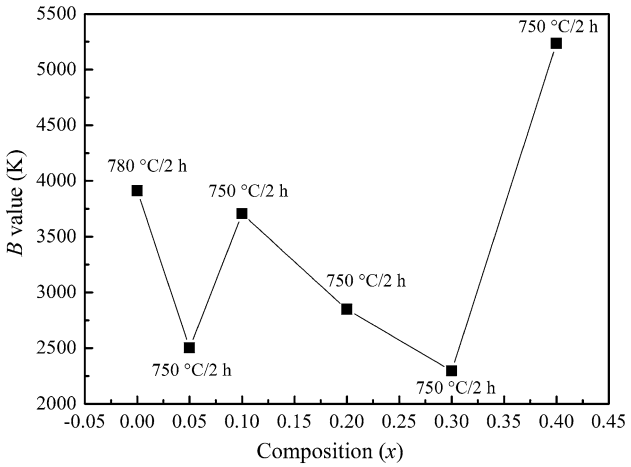

Fig. 5 B values of xMn/Co/Ni + $(1-x)$BaBiO$_3$ (x = 0.0–0.4) ceramic samples sintered at different temperatures for 2 h

the electrical conductivity for the x = 0.3 and 0.4 samples, and thus they still show good NTC temperature-sensitive behavior with the increase in measured temperature. On the other hand, Fig. 4b shows the relationship of ln(ρ) versus 1000/T for the xMn/Co/Ni + $(1-x)$BaBiO$_3$ (x = 0.0–0.4) NTC thermistors in the temperature range between 298 and 358 K. It is found that a nearly linear dependence relation exists between these two parameters for all of the samples, indicating typical NTC thermistor characteristics as well.

Figure 5 represents the composition dependence of the $B_{25/85}$ values for the xMn/Co/Ni + $(1-x)$BaBiO$_3$ (x = 0.0–0.4) ceramic samples. Therein, the $B_{25/85}$ values are calculated by Eq. (1) as 3912 K, 2503 K, 3707 K, 2848 K, 2297 K and 5235 K for the samples of x = 0.00, x = 0.05, x = 0.1, x = 0.2, x = 0.3 and x = 0.4, respectively. The $B_{25/85}$ value of these samples can be adjusted to between 2297 and 5235 K, showing that the Mn/Co/Ni-modified BaBiO$_3$ ceramic system is an interesting and practical material because the B value within the range of 2000–7000 K is desirable for the applications of NTC thermistors [33]. In fact, a B constant indicates a sensitivity to temperature excursions and is given by $B = q/k_B$, where q is the activation energy for electrical conduction and k_B is the Boltzmann constant, which is closely related to the activation energy for hopping conduction (E_a) [22]. In addition, the B value is also related to the temperature coefficient of resistance (α_T), which is given by the expression: $\alpha_T = (1/\rho)d\rho/dT = -B/T^2$ [21, 34]. The resistivity at 25 °C and 85 °C, $B_{25/85}$, E_a and α_{25} for NTC thermistors is listed in Table 2. This table indicates that the electrical properties of xMn/Co/Ni + $(1-x)$BaBiO$_3$ NTC thermistors are strongly dependent on the amount of Mn-, Co- and Ni-ions substitutions. Therein, the lower ρ_{25} value of about 760 Ω cm corresponds to the appropriate α_{25} value of -2.82% K^{-1}, which means a better NTC resistance behavior and a practical sensitivity for the sample with x = 0.05. In addition, the values of E_a in these samples with x = 0.0–0.3 vary between 0.198 and 0.337 eV, and this is within the requirements for industrial NTC thermistors (ρ_{25}: 0–12 kΩ cm and E_a: 0.1–0.2 eV), especially for temperature sensors and infrared-detecting applications [14, 35, 36].

4 Conclusion

Different amounts of Mn/Co/Ni-ions doped in BaBiO$_3$ ceramics with the formula x[(3-y-z)Mn/yCo/zNi-ions] + $(1-x)$BaBiO$_3$ (x = 0.0–0.4, y = 0.96 and z = 0.48) were prepared using a conventional solid state reaction. The structures and NTC electrical properties of as-sintered xMn/Co/Ni + $(1-x)$BaBiO$_3$ (x = 0.0–0.4) were investigated in detail. X-ray diffraction (XRD) analyses revealed that the mixture phases presented in the xMn/Co/Ni + $(1-x)$BaBiO$_3$ (x = 0.05–0.2) compounds were a major monoclinal BaBiO$_3$

Table 2 ρ_{25}, ρ_{85}, $B_{25/85}$, E_a and α_{25} of xMn/Co/Ni + $(1-x)$ $BaBiO_3$ ($x = 0.0$–0.4) composite ceramics

Sample	Sintering temperature (°C)	ρ_{25}(Ω cm)	ρ_{85}(Ω cm)	$B_{25/85}$(K)	E_a (eV)	a_{25}(%K^{-1})
$x = 0.0$	780	1300	144	3912	0.337	−4.41
$x = 0.05$	750	760	186	2502	0.216	−2.82
$x = 0.1$	750	1770	220	3707	0.319	−4.17
$x = 0.2$	750	1950	393	2848	0.245	−3.21
$x = 0.3$	750	11,720	3220	2297	0.198	−2.59
$x = 0.4$	750	1,620,000	85,300	5235	0.451	−5.90

phase and a secondary hexagonal phase of Ba(Mn, Co, Ni)O_3 isomorphic to $BaMnO_3$. In addition, the main crystalline phase changed from a monoclinic $BaBiO_3$ phase into a rhombohedral $Bi_{8.11}Ba_{0.89}O_{13.05}$ phase at $x = 0.3$, and the phase content of $Bi_{8.11}Ba_{0.89}O_{13.05}$ had a significant increase when the x value increased to 0.4. The EDS results also verified the correctness of the phase compositions on the XRD pattern analysis results. With respect to electrical properties, the sample with $x = 0.05$ showed a moderate $B_{25/85}$ value (~2502 K) and lower room temperature resistivity (ρ_{25} = ~760 Ω cm) compared to those of $BaBiO_3$ (~3912 K and ~1300 Ω cm). As $x = 0.4$, there was a sharp increase in the ρ_{25} value of ~1620 kΩ cm, and it was strongly related with the changes in crystal structures and the decrease in charge carrier concentration. These results also illustrated that the electrical properties of the xMn/Co/Ni + $(1-x)$ $BaBiO_3$ NTC thermistors could be adjusted by regulating the Mn/Co/Ni-doped amount. In summary, the $B_{25/85}$ and ρ_{25} values in the present NTC thermistor ceramic systems are in the range of 2297–5235 K and 760 Ω cm–1620 kΩ cm, respectively, which implies that the Mn/Co/Ni-modified $BaBiO_3$-based ceramic systems provide considerable flexibility and feasibility as potential candidates for tailoring of electrical properties, and this will apply to NTC thermistor applications with varying performance requirements.

Acknowledgements Financial support from the National Natural Science Foundation of China (Grants Nos. 51462005 and 61561011) is gratefully acknowledged by the authors.

References

1. H. Han, S. Mhin, K.R. Park, K.M. Kim, J.I. Lee, J.H. Ryu, Fe doped Ni-Mn-Co-O ceramics with varying Fe content as negative temperature coefficient sensors. Ceram. Int. **43**, 10528–10532 (2017)
2. G. Na, Y.D. Li, Effects of Cd and Cd–Cu doping on the microstructure and electrical properties of NiMnCoO NTC ceramics, Adv. Mater. Res. **1632**, 236–238 (2011)
3. A. Feteira, Negative temperature coefficient resistance (NTCR) ceramic thermistors: an industrial perspective. J. Am. Ceram. Soc. **92**, 967–983 (2009)
4. E. Rios, J.L. Gautier, G. Poillerat, P. Chartier, Mixed valency spinel oxides of transition metals and electrocatalysis: case of the $Mn_xCo_{3-x}O_4$ system. Electrochim. Acta **44**, 1491–1497 (1998)
5. C. Peng, H. Zhang, A. Chang, F. Guan, B. Zhang, P. Zhao, Effect of Mg substitution on microstructure and electrical properties of $Mn_{1.25}Ni_{0.75}Co_{1.0-x}Mg_xO_4$ ($0 \le x \le 1$) NTC ceramics. J. Mater. Sci.: Mater. Electron. **23**, 851 (2012)
6. K. Park, J.K. Lee, The effect of ZnO content and sintering temperature on the electrical properties of Cu-containing $Mn_{1.95-x}Ni_{0.45}Co_{0.15}Cu_{0.45}Zn_xO_4$ ($0 \le x \le 0.3$) NTC thermistors. J. Alloys Compd. **475**, 513–517 (2009)
7. S.A. Kanade, V. Puri, Electrical properties of thick-film NTC thermistor composed of $Ni_{0.8}Co_{0.2}Mn_2O_4$ ceramic: effect of inorganic oxide binder. Mater. Res. Bull **43**, 819–824 (2008)
8. A.V. Salker, S.M. Gurav, Electronic and catalytic studies on $Co_{1-x}Cu_xMn_2O_4$ for CO oxidation. J. Mater. Sci. **35**, 4713–4719 (2000)
9. Z.B. Wang, C.H. Zhao, P.H. Yang, A.J.A. Winnubst, C.S. Chen, X-ray diffraction and infrared spectra studies of $Fe_xMn_{2.34-x}Ni_{0.66}O_4$ ($0 < x < 1$) NTC ceramics. J. Eur. Ceram. Soc. **26**, 2833–2837 (2006)
10. S. Mhin, H. Han, D. Kim, S. Yeo, J.I. Lee, J.H. Ryu, Phase evolution of (Ni, Co, Mn)O_4 during heat treatment with high temperature in situ X-ray diffraction. Ceram. Int. **42**, 5412–5417 (2016)
11. H. Han, J.S. Lee, J.H. Ryu, K.M. Kim, J.L. Jones, J. Lim, S. Guillemet-Fritsch, H.C. Lee, S. Mhin, Effect of high cobalt concentration on hopping motion in cobalt manganese spinel oxide ($Co_xMn_{3-x}O_4$, $x \ge 2.3$). J. Phys. Chem. C **120**, 13667–13674 (2016)
12. M.Y. Guan, J.C. Yao, W.W. Kong, J.H. Wang, A.M. Chang, Effects of Zn-doped on the microstructure and electrical properties of $Mn_{1.5-x}Co_{1.2}C_{u0.3}Zn_xO_4$ ($0 \le x \le 0.5$) NTC ceramics. J. Mater. Sci.: Mater. Electron. **29**, 5082–5086 (2018)
13. R. Dannenberg, S. Baliga, R.J. Gambino, A.H. King, A.P. Doctor, Resistivity, thermopower and the correlation to infrared active vibrations of $Mn_{1.56}Co_{0.96}Ni_{0.48}O_4$ spinel films sputtered in an oxygen partial pressure series. J. Appl. Phys. **86**, 514–523 (1999)
14. Y.Q. Gao, Z.M. Huang, Y. Hou, J. Wu, W. Zhou, C. OuYang, J.G. Huang, J.C. Tong, J.H. Chu, Structural and electrical properties of $Mn_{1.56}Co_{0.96}Ni_{0.48}O_4$ NTC thermistor films. Mat. Sci. Eng. B. **185**, 74–78 (2014)
15. W.W. Kong, H.J. Bu, B. Gao, L. Chen, F. Cheng, P.J. Zhao, G. Ji, A.M. Chang, C.P. Jiang, Effects of preferred orientation on electrical properties of $Mn_{1.56}Co_{0.96}Ni_{0.48}O_{4\pm\delta}$ spinel films. Mater. Lett **137**, 36–40 (2014)
16. R. Schmidt, A. Basu, A.W. Brinkman, Z. Klusek, P.K. Datta, Electron-hopping modes in $NiMn_2O_{4+\delta}$ materials. Appl. Phys. Lett. **86**, 073501 (2005)
17. H.M. Zhang, A.M. Chang, C.W. Peng, Preparation and characterization of Fe^{3+}-doped $Ni_{0.9}Co_{0.8}Mn_{1.3-x}Fe_xO_4$ ($0 \le x \le 0.7$) negative temperature coefficient ceramic materials. Microelectron. Eng **88**, 2934–2940 (2011)

18. J. Guo, H. Zhang, Z.L. He, S.H. Li, Z.C. Li, Electrical properties and temperature sensitivity of Mo-modified $MnFe_2O_4$ ceramics for application of NTC thermistors. J. Mater. Sci. **29**, 2491–2499 (2018)
19. C.J. Ma, H. Gao, Preparation and characterization of single-phase $NiMn_2O_4$ NTC ceramics by two-step sintering method. J. Mater. Sci. **28**, 6699–6703 (2017)
20. C.P. Huang, L. Chen, Q.A. Zhang, S.N. Chang, B. Zhang, A.M. Chang, H.M. Zhang, Preparation and characterization of $LaMn_{0.5}Co_{0.5}O_3$-$Ni_{0.66}Mn_{2.34}O_4$ composite NTC ceramics. J. Mater. Sci. **27**, 7560–7565 (2016)
21. C.J. Ma, Y.F. Liu, Y.N. Lu, H. Qian, Preparation and electrical properties of $Ni_{0.6}Mn_{2.4-x}Ti_xO_4$ NTC ceramics. J. Alloys Compd. **650**, 931–935 (2015)
22. B. Zhang, Q. Zhao, A.M. Chang, X. Huang, J. Hou, P.J. Zhao, G. Ji, La_2O_3-doped $0.6Y_2O_3 - 0.4YCr_{0.5}Mn_{0.5}O_3$ composite NTC ceramics for wide range of temperature sensing. J. Alloys Compd. **581**, 573–578 (2013)
23. Z.Y. Guo, J.M. Shao, H. Lin, M.D. Jiang, S.Y. Chen, Z.C. Li, Electrical conductivity and temperature sensitivity of ceramics based on NiO simple oxides for NTC applications. J. Mater. Sci. **28**, 11871–11877 (2017)
24. B. Zhang, Q. Zhao, C.J. Zhao, A.M. Chang, Comparison of structure and electrical properties of vacuum-sintered and conventional-sintered $Ca_{1-x}Y_xCeNbWO_8$ NTC ceramics. J. Alloys Compd. **698**, 1–6 (2017)
25. X.Q. Li, Y. Luo, X.Y. Liu, Preparation and electrical properties of perovskite ceramics in the system $BaBi_{1-x}Sb_xO_3$ ($0 \le x \le 0.5$). J. Alloys Compd. **509**, 5373–5375 (2011)
26. Y. Luo, X.Y. Liu, X.Q. Li, Electrical properties of $BaTiO_3$-based NTC thermistors doped by $BaBiO_3$ and La_2O_3. J. Mater. Sci. **17**, 909–913 (2006)
27. Y. Luo, X.Y. Liu, G.H. Chen, Effect of Y_2O_3 addition on the electrical properties of $BaTiO_3$-based NTC thermistors. Mater. Lett **60**, 1011 (2006)
28. R.D. Shannon, Revised effective ionic radii and systematic studies of interatomic distances in halides and chalcogenides. Acta. Cryst. A **32**, 751–767 (1976)
29. M. Nagoshi, T. Suzuki, Y. Fukuda, K. Ueki, A. Tokiwa, M. Kiruchi, Y. Syono, M. Tachiki, Electronic states of $BaBiO_3$- delta and K-doping effects studied by photoelectron spectroscopy. J. Phys.: Condens. Matter. **4**(26), 5769 (1992)
30. Z.N. Akhtar, M.J. Akhtar, C.R.A. Catlow, X-ray absorption near-edge studies of $BaBiO_3$, $BaBi_{1-x}Pb_xO_3$ and $Ba_{1-x}K_xBiO_3$ systems. J. Phys. **5**, 2643 (1992)
31. H. Han, H. Lee, J. Lim, K.M. Kim, Y.R. Hong, J. Lee, J. Forrester, J.H. Ryu, S. Mhin, Hopping conduction in (Ni, Co, Mn) O_4 prepared by different synthetic routes: conventional and spark plasma sintering. Ceram. Int. **43**, 16070–16075 (2017)
32. K. Park, D.Y. Bang, Electrical properties of Ni–Mn–Co–(Fe) oxide thick-film NTC thermistors prepared by screen printing. J. Mater. Sci. **14**(2), 81–87 (2003)
33. K. Park, S.J. Yun, Influence of the composition on the electrical properties of $(Mn_{2.1-x}Ni_{0.9}Si_x)O_4$ negative temperature coefficient thermistors. J. Mater. Sci. **15**, 359–362 (2004)
34. K. Park, J.K. Lee, Mn-Ni-Co-Cu-Zn-O NTC thermistors with high thermal stability for low resistance applications. Scr. Mater **57**, 329–332 (2007)
35. P. Umadevi, C.L. Nagendra, Preparation and characterisation of transition metal oxide micro-thermistors and their application to immersed thermistor bolometer infrared detectors. Sens. Actuators A **96**, 114–124 (2002)
36. C.J. Ma, Y.F. Liu, Y.N. Lu, Preparation routes and electrical properties for $Ni_{0.6}Mn_{2.4}O_4$ NTC ceramics. J. Mater. Sci. **26**, 7238 (2015)